

Locomotion Efficiency of Underwater Snake Robots with Thrusters

E. Kelasidi, K. Y. Pettersen, P. Liljebäck and J. T. Gravdahl

Abstract—Lately there has been an increasing interest for subsea inspection and intervention tasks, and in particular on solutions which combine smaller size, increased flexibility and maneuverability, and decreased cost. Biologically inspired underwater snake robots (USRs) can provide both inspection and intervention capabilities and are thus interesting candidates for the next generation inspection and intervention vehicles. In this paper, we focus on a new type of USR equipped with thrusters, which combine the flexibility and maneuverability of conventional USRs with the locomotion capabilities of traditional marine vessels with thrusters. This vehicle configuration represents a promising solution for operations inside narrow and restricted parts of subsea structures. The paper considers the locomotion efficiency of this new type of USR with thrusters by experimentally investigating fundamental properties of the velocity and the power consumption of a USR with and without thrusters, both for lateral undulation and eel-like motion.

I. INTRODUCTION

For several decades autonomous underwater vehicles (AUVs) and remotely operated vehicles (ROVs) have been widely used for different challenging subsea tasks [1]. Recently, the bio-robotics community has investigated a bio-inspired underwater snake-like robotic solution as an interesting alternative to conventional ROVs and AUVs. These biologically inspired systems have a long, slender and flexible body which gives them the ability to reach and operate in locations not accessible by larger and more conventional ROVs and AUVs. USRs thus bring a promising prospective to improve the efficiency and maneuverability of modern-day underwater vehicles [2], [3], [4], [5]. A large variety of snake-like robots have been developed over the years. A review of land-based snake-like robots can be found in [6]. The work of Hirose [7], one of the first approaches to develop a snake robot, is essential. While a variety of different snake-like robots have been constructed since then, only a few working examples of swimming snake robots currently exist. These include the eel robots REEL I [8] and II [9], the lamprey robot built at Northeastern University [10], AmphiBot I [11], AmphiBot II [12] and AmphiBot III [13] from the EPFL lab, Perambulator III [14], the amphibious snake robot ACM 5 [15], [16], the HELIX-I [17], a biorobotic platform inspired by the lamprey [18], and the underwater snake

robot Mamba, recently developed by the authors at NTNU in Norway [19]. The concept of an underwater swimming manipulator (USM), which is a hyper-redundant AUV with the potential to replace traditional ROVs and AUVs for routine inspection and lighter intervention tasks, is presented in [20]. In this paper, the authors study a particular case of USMs, namely the underwater snake robot Mamba with thrusters attached at the tail module of the robot. The tail thrusters induce linear forces along the body which increase the overall velocity of the robot. A control framework for USMs equipped with thrusters is presented in [21]. To the authors' best knowledge, this is the first developed USR which combines the undulatory motion of a bio-inspired USR with thrusters.

In order to realize fully operational USRs for subsea applications, there is a need for addressing the locomotion efficiency of such vehicles. In particular, an autonomous USR (without an external power supply cable) can only carry a limited amount of onboard power (batteries). Its usefulness as an autonomous subsea vehicle thus relies on its ability to move energy efficiently under water. In [22], the relationships between the achieved forward velocity, the consumed energy, and the parameters of the gait patterns were investigated for USRs. In addition, empirical rules were proposed in order to choose the most efficient motion pattern. In [23], a simulation study was undertaken in order to compare the power consumption of swimming snake robots with that of today's benchmark solution for subsea inspection, maintenance and repair, which are ROVs. The presented simulation results showed that a USR is more energy efficient than a ROV for all the compared motion modes. Note that in [23] the joints are assumed to be ideal since a detailed model of the servos are not considered. By using nonlinear averaging theory, in [24], fundamental properties are derived regarding the relationship between the gait parameters and the forward velocity. [25] investigates experimentally the validity of the empirical rules proposed in [22], [23] regarding the relationship between the gait parameters, the velocity and the power consumption using a physical USR [19]. Furthermore, [26] proposed a multi-objective optimization scheme to obtain optimal gait parameters for USRs. To our knowledge, however, no research has been published investigating experimentally the locomotion efficiency of the new type of USRs that are equipped with thrusters. To this end, this paper presents and experimentally investigates several fundamental properties of the velocity and the power consumption of an underwater snake robot with and without thrusters, both for lateral undulation and eel-like motion patterns for forward motion. In particular,

E. Kelasidi, K. Y. Pettersen and P. Liljebäck are with the Centre for Autonomous Marine Operations and Systems, Dept. of Engineering Cybernetics at NTNU, NO-7491 Trondheim, Norway. E-mail: {Eleni.Kelasidi,Kristin.Y.Pettersen,Pal.Liljeback}@itk.ntnu.no

J. T. Gravdahl is with the Dept. of Engineering Cybernetics at NTNU, NO-7491 Trondheim, Norway. E-mail: Tommy.Gravdahl@itk.ntnu.no

Research partly funded by VISTA - a basic research program in collaboration between The Norwegian Academy of Science and Letters, and Statoil, and partly supported by the Research Council of Norway through its Centres of Excellence funding scheme, project no. 223254-NTNU AMOS.



Fig. 1: Mamba with and without thrusters.

we present experimental results regarding the relationship between the parameters of the gait patterns, the forward velocity and the power consumption for different configurations of the swimming robot both with and without the use of thrusters.

The paper is organized as follows. Section II presents the USR Mamba equipped with thrusters, and the force mapping from the control inputs to the actual thruster forces. The experimental investigation of locomotion efficiency is presented in Section III. Finally, conclusions and suggestions for future research are given in Section IV.

II. UNDERWATER SNAKE ROBOT WITH THRUSTERS

In this section we present the underwater snake robot Mamba with thrusters and the experimental setup used for mapping the control inputs to the forces produced by the thruster modules attached at the tail of the robot. A more detailed description of the robot without the thruster module at the tail can be found in [19].

A. The underwater snake robot Mamba with thrusters

The USR Mamba with and without thrusters (Fig. 1) has recently been developed by the authors to investigate different types of underwater locomotion. The robot is watertight down to about 5 m and it has a modular design with a common mechanical and electrical interface between the modules. Each joint module is actuated by a Hitec servo motor (HSR 5990TG) and contains two temperature sensors, a 3-axis accelerometer, and a water leakage detector. Furthermore, each joint is controlled by a microcontroller card (TITechSH2 Tiny Controller from HiBot), and all microcontrollers in the robot communicate over a CAN bus. Power supply cables (35 V) run through all the modules along with the CAN bus. The robotic platform also includes a tail thruster module with two 400HFS-L thrusters from CrustCrawler, as shown in Fig. 2.

The configuration of the robot used for the experimental results presented in Section III consisted of 18 identical joint modules mounted horizontally and vertically in an alternating fashion [19]. During the experiments we covered the robot by a watertight skin in order to achieve an additional water barrier (Fig. 1). The skin was custom designed from Groundsheet, Nylon, PU-coated, 120 g/m² material, and is sealed at the head and the tail parts using rubber bottle wrist seals, which are glued to the skin. Note that this type of cover

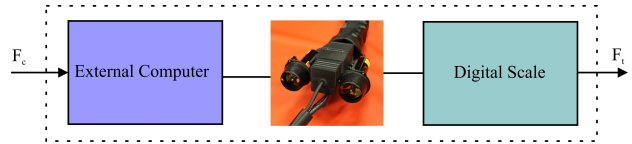


Fig. 2: Illustration of the setup for force mapping.

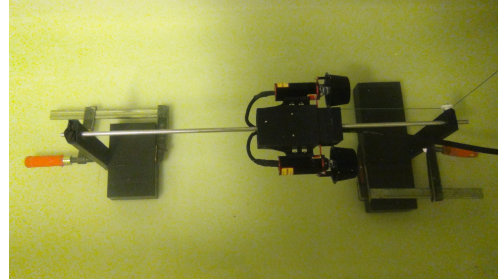


Fig. 3: Setup for mapping the control inputs u_c to thruster forces F_t .

makes the robot's outer surface more smooth, thus reducing drag effects.

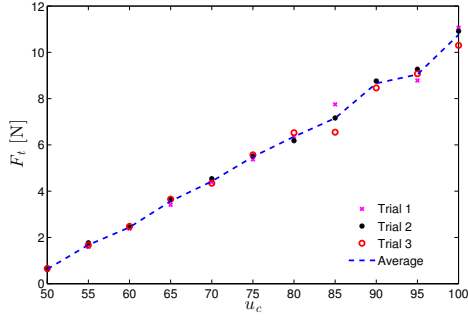
B. Mapping from control inputs to thruster forces

In order to study the energy efficiency of Mamba with thrusters, it is important to know the amplitude of the applied thruster forces as a function of the particular control inputs. The thruster module was controlled by a microcontroller programmed such that a control input in the range 0 - 100 controlled the speed of the thruster between zero and maximum. In this section we present the experimental setup used for determining the mapping from these control inputs, denoted by u_c , to the forces produced by the thrusters at the tail of the robot, and also the obtained mapping results. As seen in Fig. 3 the thruster module was attached to a straight smooth rod, and was able to move along the rod while being fully submerged in a basin. In the experiments, we used a digital scale in order to measure the force produced from the applied control inputs. The digital scale was attached to the back of the thruster module using a pulley. In particular, the control inputs, u_c , were sent from a computer running Labview to the thruster module, and afterwards the digital scale was observed to obtain the thruster forces F_t . We used a video camera recording to obtain the values measured by the digital scale.

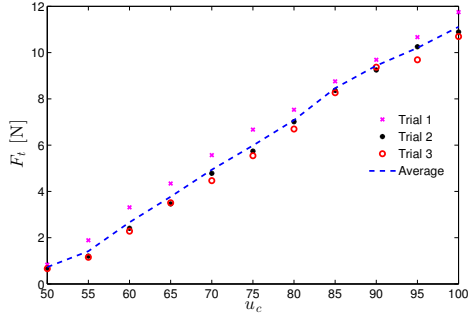
Fig. 4 shows the experimental results of the force mapping. Note that initially we performed three trials for each control input, obtaining subsequently three measurements for each value of the control input u_c as shown in Fig. 4a. Furthermore, we performed three different experiments by continuously increasing the values of the control input u_c from 50 to 100 (Fig. 4b). In all the cases, we see that the mapping between the control inputs and the thruster forces is quite linear, and the repeatability of the results is clearly shown in Fig. 4.

III. EXPERIMENTAL INVESTIGATION OF LOCOMOTION EFFICIENCY

In this section we investigate the energy efficiency of the underwater snake robot Mamba with and without thrusters



(a) Discrete trials for force mapping



(b) Monotonically increasing force mapping

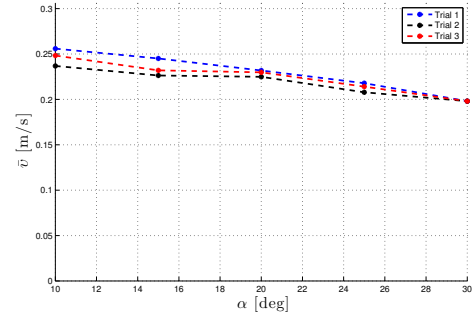
Fig. 4: Mapping from control inputs to thruster forces.

at the tail module. First, we describe the experimental setup employed for the investigation of the relationship between the gait patterns, the forward velocity and the power consumption for a new type of USR with thrusters. Then we present the experimental results.

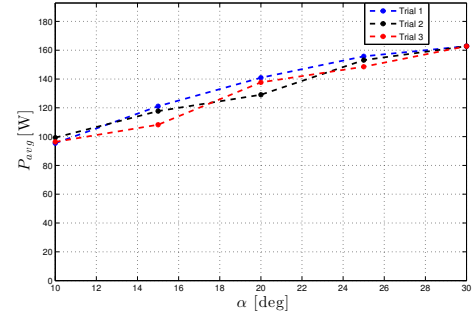
A. Experimental setup

The experiments were performed in the MC-lab in Marintek, Trondheim, Norway [27], in a tank of dimensions L: 40 m, H: 1.5 m and W: 6.45 m. The camera system from Qualisys [28] installed at MC-lab consists of six identical underwater cameras providing a working area of dimensions $12\text{m} \times 1.35\text{m} \times 5.45\text{m}$ for real time measurements of the position and the orientation of the robot.

The underwater snake robot Mamba with and without thrusters, which is presented in Section II.A, was used for the experiments. Note that the results presented in this paper are obtained for horizontal motion of the robot, and thus the joint angles responsible for the vertical motion were set to zero degrees. Reflective markers were attached at the tail part of the robot, as shown in Fig. 8, for real time tracking of the position and the orientation of the tail link in the global frame. Afterwards, the position of the center of mass (CM), \mathbf{p}_{CM} , and the absolute link angles, θ , were calculated using the kinematic equations by combining the measured position and the orientation of the tail link and the individual joint angles. For more details regarding the experimental setup see [29].

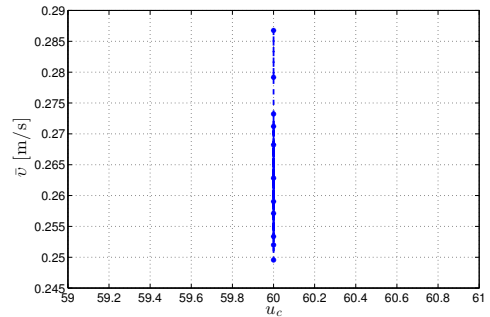


(a) Forward velocity for $\omega = 90^\circ/\text{s}$ and $\delta = 30^\circ$.

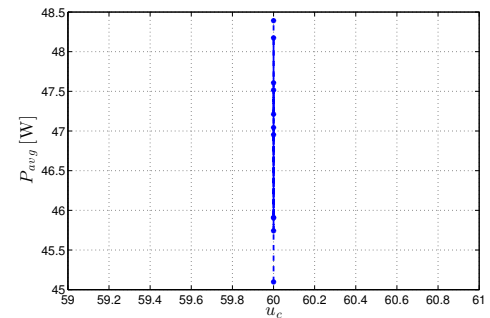


(b) Average power consumption for $\omega = 90^\circ/\text{s}$ and $\delta = 30^\circ$.

Fig. 5: Results for the USR using thrusters combined with lateral undulation motion pattern for $u_c = 60$.

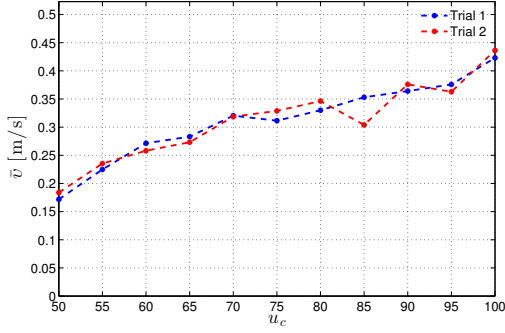


(a) Forward velocity.

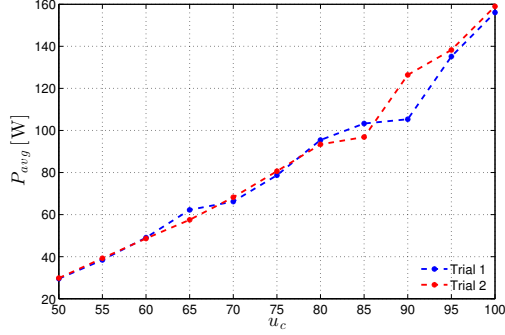


(b) Average power consumption.

Fig. 6: Results for the USR using only thrusters at the tail part for propulsion for same u_c .



(a) Forward velocity.



(b) Average power consumption.

Fig. 7: Results for the USR using only thrusters at the tail part for propulsion for different values of u_c .

B. Energy Efficiency

For USRs without thrusters, the propulsion is generated by the motion of the joints and the corresponding interaction between the robot body and the surrounding fluid, while for a USR with thrusters the propulsion is generated by the combined motion of the joints and the thruster modules.

For the experimental results presented in this paper, the average power consumption is calculated by using the following equation

$$P_{\text{avg}} = VI_{\text{avg}}, \quad (1)$$

where $V = 35$ [V] and I_{avg} [A] is the average current that is measured using the high performance industrial logging multimeter FLUKE 289 [30]. The multimeter was connected to the power box on the tip of the power supply cable that is used for our experiments with Mamba. The current values were obtained for a wide range of the values for the gait parameters for two motion patterns: lateral undulation and eel-like motion. In particular, we measured the average, the maximum and the minimum values of the current for a certain time.

The CM position of the robot was calculated as described in Section III.B, while the average forward velocity for each experimental trial was calculated as

$$\bar{v} = \frac{\sqrt{(p_{\text{stop},x} - p_{\text{start},x})^2 + (p_{\text{stop},y} - p_{\text{start},y})^2}}{t_{\text{stop}} - t_{\text{start}}}, \quad (2)$$

where $\mathbf{p}_{\text{start}}$ and \mathbf{p}_{stop} represent the initial and the final points of the distance travelled in the time interval $t_{\text{stop}} - t_{\text{start}}$.

TABLE I: Comparison results for the locomotion efficiency of a USR using thrusters and lateral undulation motion pattern.

	max \bar{v} [m/s]	max P_{avg} [W]	min \bar{v} [m/s]	min P_{avg} [W]
Case 1	0.2713	49.0490	0.2581	48.6220
Case 3 for different values of α	0.2558	162.8200	0.1981	95.4345
Case 3 for different values of ω	0.2184	175.0700	0.1772	113.2600
Case 3 for different values of δ	0.2358	146.2650	0.1871	77.8820
Case 2	0.4362	158.9875	0.4229	156.1000
Case 4 for different values of α	0.4439	250.9850	0.3646	190.8550
Case 4 for different values of ω	0.4137	259.6300	0.3433	62.5800
Case 4 for different values of δ	0.4302	230.3210	0.3778	180.4250
Case 5 for different values of α	0.0768	123.0950	0.0254	72.3870
Case 5 for different values of ω	0.0975	136.8500	0.0732	80.0100
Case 5 for different values of δ	0.0711	118.7550	0.0317	41.4330

TABLE II: Comparison results for the locomotion efficiency of a USR using thrusters and eel-like motion pattern.

	max \bar{v} [m/s]	max P_{avg} [W]	min \bar{v} [m/s]	min P_{avg} [W]
Case 1	0.2713	49.0490	0.2581	48.6220
Case 6 for different values of α	0.2746	158.2035	0.2154	83.7725
Case 6 for different values of ω	0.2318	158.2035	0.2053	110.1975
Case 6 for different values of δ	0.2494	158.2035	0.2154	85.9215
Case 2	0.4362	158.9875	0.4229	156.1000
Case 7 for different values of α	0.4189	239.1200	0.4023	178.1150
Case 7 for different values of ω	0.4460	247.8700	0.4098	213.2900
Case 7 for different values of δ	0.4268	239.1200	0.4001	184.9400
Case 8 for different values of α	0.0417	96.4250	0.0186	49.6720
Case 8 for different values of ω	0.0589	101.1885	0.0350	73.2970
Case 8 for different values of δ	0.0561	98.0315	0.0344	49.0175

The experimentally obtained properties for the gait parameters in this paper hold for USRs that follow a combined sinusoidal motion pattern and thrusters propulsive modules. As shown in [29], a general sinusoidal motion pattern can be achieved by making each joint $i \in \{1, \dots, n-1\}$ of the robot track the following reference signal

$$\phi_i^*(t) = \alpha g(i, n) \sin(\omega t + (i-1)\delta) + \phi_0, \quad (3)$$

where α , ω and δ represent the amplitude, the frequency and the phase shift between the joints, respectively. The parameter ϕ_0 is a joint offset that induces turning motion and n stands for the number of links of the robot [29]. The scaling function $g(i, n)$ is responsible for scaling the joint amplitude along the body of the robot, which allows (3) to describe a quite general class of sinusoidal functions. In particular, by choosing $g(i, n) = 1$ it is possible to obtain the motion pattern lateral undulation, and by choosing $g(i, n) = (n-i)/(n+1)$ the eel-like motion pattern is achieved.

The thrusters were controlled via Labview by sending

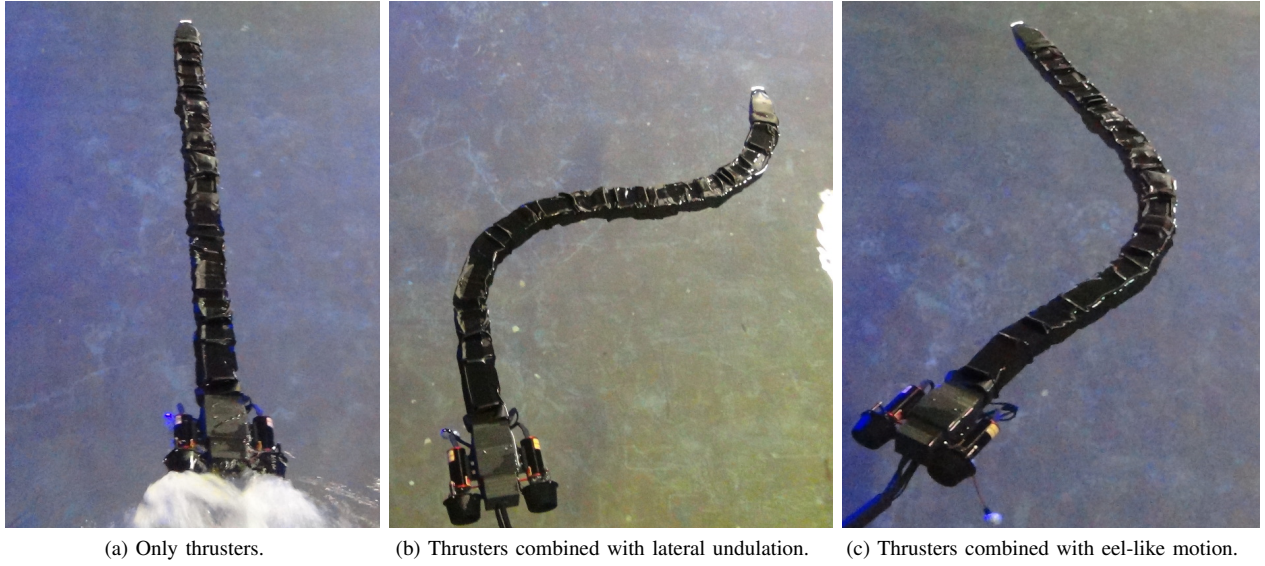


Fig. 8: Experimental case studies with the underwater snake robot Mamba.

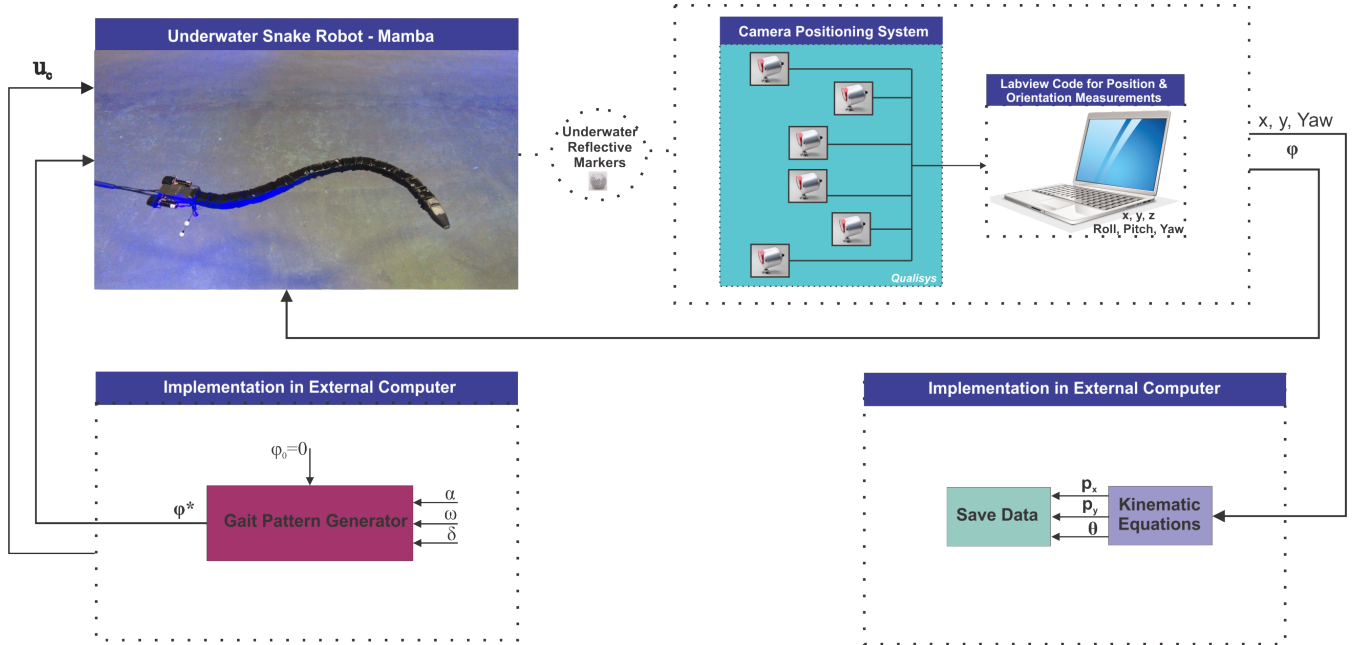


Fig. 9: Illustration of the experimental setup.

the control inputs directly to the low level controller implemented for the thrusters module. The mapping between the control inputs and the resulting thruster forces was known from the experiments described in Section II.B. An illustration of the experimental process that was followed in order to obtain the results presented in this paper, is shown in Fig. 9.

C. Experimental results

During the experiments we applied a sinusoidal motion patterns based on (3). We investigated the locomotion efficiency for different values of the gait parameters, both for lateral undulation and eel-like motion patterns. In particular, in each trial, the reference joint angles for $n = 10$, were computed by (3) and sent to the robot via the CAN. For

each trial the average forward velocity was calculated by (2) for approximately 15 sec of motion. Note that the initial values of the link angles were set to zero before each trial.

In this section we present results regarding the achieved forward velocity and the average power consumption for the following different configurations of the robot:

- **Case 1**—for control input $u_c = 60$,
- **Case 2**—for control input $u_c = 100$,
- **Case 3**—for control input $u_c = 60$ combined with lateral undulation,
- **Case 4**—for control input $u_c = 100$ combined with lateral undulation,
- **Case 5**—for control input $u_c = 0$ combined with lateral undulation,

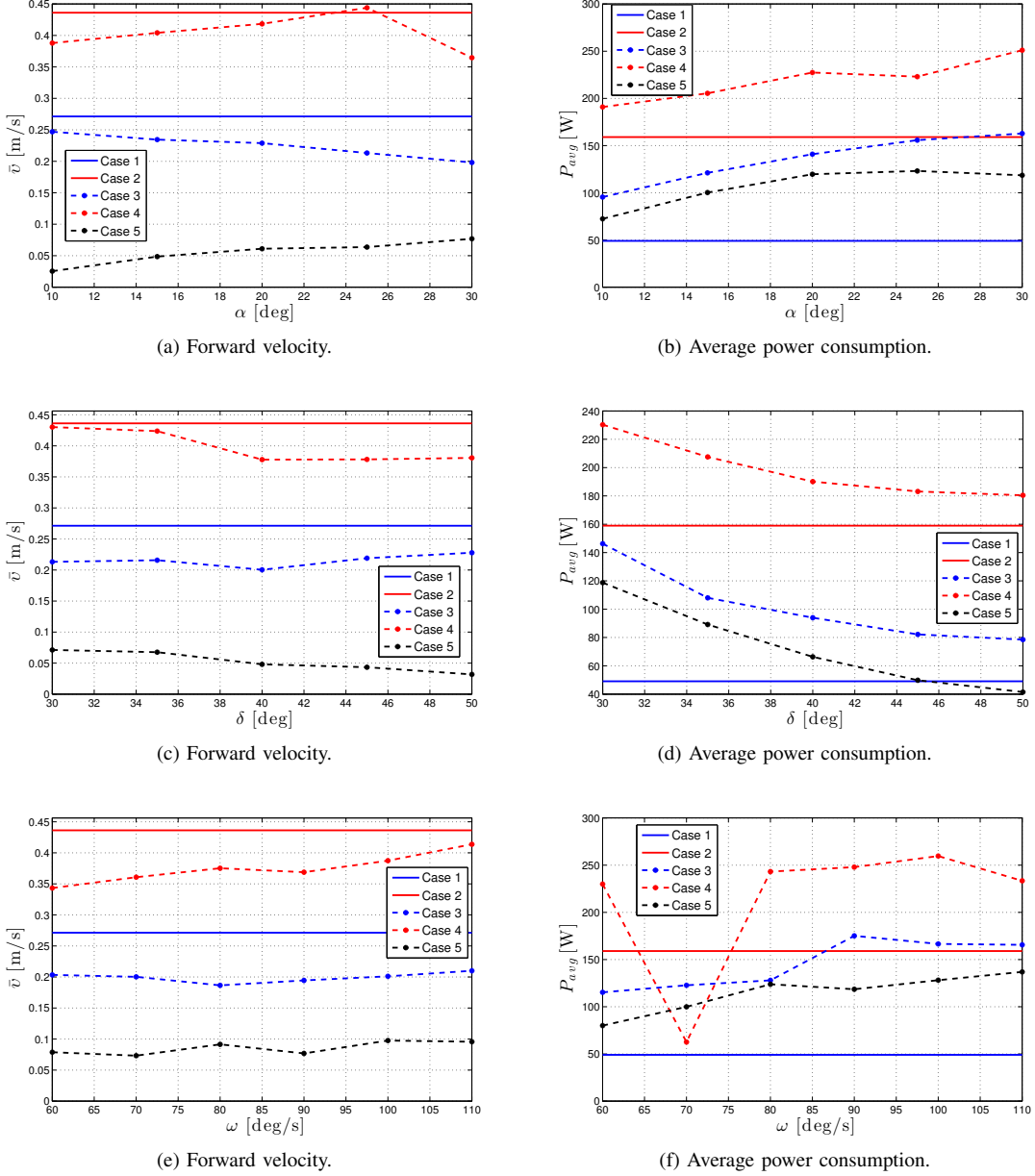


Fig. 10: Comparison results for the USR with thrusters for lateral undulation motion pattern.

- **Case 6**—for control input $u_c = 60$ combined with eel-like motion pattern,
- **Case 7**—for control input $u_c = 100$ combined with eel-like motion pattern and
- **Case 8**—for control input $u_c = 0$ combined with eel-like motion pattern.

In particular, we have performed experiments for a quite wide range of values of the gait parameters α , ω and δ , both for lateral undulation and eel-like motion. For Cases 3-8, we have obtained three trials of measurements in order to investigate the repeatability of the performed experiments. In particular, Fig. 5 shows the results of the three trials for Case 3 for all the investigated values of the gait parameter α , and we can clearly see that for all the trials both for the average forward velocity and the power consumption the obtained

results are similar. In addition, Fig. 6 shows several trials for Case 1 where the locomotion efficiency is investigated using only thrusters, and as we can see the error between the different trials is negligible despite the inevitable noise on the measurements from the different sensors used for the experiments, thus demonstrating repeatability.

Experimental results for the USR Mamba using only thrusters for propulsion is presented in Fig. 7 for different values of u_c . From this figure, we can see that for both trials the average forward velocity and the power consumption are increased by increasing u_c . Furthermore, we have obtained comparison results for all the different cases, both for lateral undulation and eel-like motion patterns, by calculating the averaged value of the different trials obtained for each case as shown in Fig. 10 and Fig. 11, respectively. From these

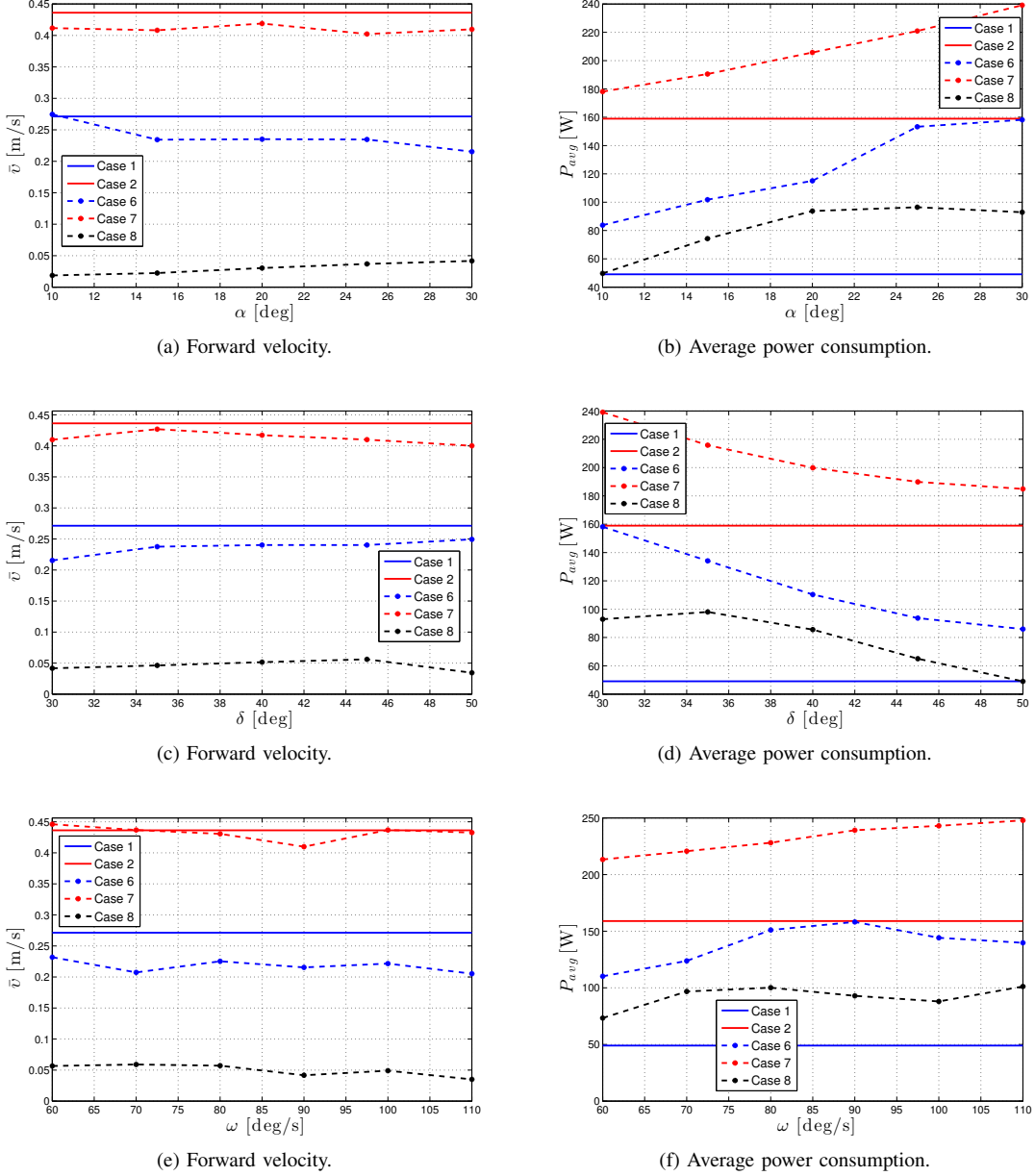


Fig. 11: Comparison results for the USR with thrusters for eel-like motion pattern.

figures, we can clearly see that the robot achieves faster motion using only the thrusters (Case 1 and Case 2). The obtained results show that the undulation does not contribute to the achieved speed while the power consumption increases significantly using the undulatory motion for a USR using servo motors for actuation of the joints. Note that the dip for Case 4 in Fig. 10f, results from that the multimeter lost the connection and we were not able to obtain results for the value $\omega = 70^\circ/\text{s}$. Table I and Table II present summarized results comparing the different investigated cases for the locomotion efficiency of Mamba with thrusters. As we can see from these obtained experimental results for Mamba, for all the cases for different values of the gait parameters α , ω and δ , except one case using thrusters with eel-like motion, the robot achieves faster motion using only thrusters and at the

same time consumes less energy than using combined motion with thrusters and joints. The experiments thus suggest that for efficient transportation, the USR with thrusters should mainly use the thrusters for locomotion, while the articulation should be used for direction control instead of using a sinusoidal motion to support the locomotion. Equipping the USR with tail thrusters thus present an important benefit for forward velocity and power consumption. Furthermore, the slender and articulated body of the USR provides significant flexibility and increases the maneuverability of the robot for subsea applications.

IV. CONCLUSIONS AND FUTURE WORK

In this paper, we presented results regarding the locomotion efficiency of a new type of USR with thrusters, by

experimentally investigating fundamental properties of the velocity and the power consumption of the USR Mamba with and without tail thrusters, both for lateral undulation and eel-like motion patterns. Experimental results show that the USR with thrusters at the tail module achieves a significant increase of the forward velocity. In particular, the obtained experimental results showed that the robot is able to achieve faster motion by using only the thrusters attached at the tail part, and at the same time it consumes less power than using the combined motion with thrusters and body undulation. The experiments thus suggest that for efficient transportation, the USR with tail thrusters should mainly use the thrusters for locomotion, while the articulation should be used for direction control instead of using the conventional USR sinusoidal motion to support the locomotion. Equipping USRs with tail thrusters thus presents an important benefit for forward velocity and power consumption. In future work, the authors will investigate also other configurations, including fins and tail to the USR design. We will also investigate several other motion patterns in addition to the two most common motion patterns investigated in this paper, in order to study the locomotion efficiency of USRs with thrusters.

ACKNOWLEDGMENT

The authors gratefully acknowledge the engineers at the Department of Engineering Cybernetics, Terje Haugen, Glenn Angell and Daniel Bogen, for implementing the necessary components for the experimental setup.

REFERENCES

- [1] T. I. Fossen, *Handbook of Marine Craft Hydrodynamics and Motion Control*. John Wiley & Sons, Ltd, 2011.
- [2] E. Kelasidi, K. Y. Pettersen, J. T. Gravdahl, and P. Liljebäck, "Modeling of underwater snake robots," in *Proc. IEEE International Conference on Robotics and Automation (ICRA)*, Hong Kong, China, May 31-June 7 2014, pp. 4540–4547.
- [3] F. Boyer, M. Porez, and W. Khalil, "Macro-continuous computed torque algorithm for a three-dimensional eel-like robot," *IEEE Transactions on Robotics*, vol. 22, no. 4, pp. 763–775, 2006.
- [4] A. Wiens and M. Nahon, "Optimally efficient swimming in hyper-redundant mechanisms: control, design, and energy recovery," *Bioinspiration & Biomimetics*, vol. 7, no. 4, p. 046016, 2012.
- [5] W. Khalil, G. Gallot, and F. Boyer, "Dynamic modeling and simulation of a 3-D serial eel-like robot," *IEEE Transactions on Systems, Man, and Cybernetics, Part C: Applications and Reviews*, vol. 37, no. 6, pp. 1259–1268, 2007.
- [6] P. Liljebäck, K. Y. Pettersen, Ø. Stavdahl, and J. T. Gravdahl, "A review on modelling, implementation, and control of snake robots," *Robotics and Autonomous Systems*, vol. 60, no. 1, pp. 29–40, 2012.
- [7] S. Hirose, *Biologically Inspired Robots: Snake-Like Locomotors and Manipulators*. Oxford University Press, 1993.
- [8] K. Melsaac and J. Ostrowski, "A geometric approach to anguilliform locomotion: modelling of an underwater eel robot," in *Proc. International Conference on Robotics and Automation (ICRA)*, Detroit, MI, May 10-15 1999, pp. 2843–2848.
- [9] K. McIsaac and J. Ostrowski, "Experiments in closed-loop control for an underwater eel-like robot," in *Proc. IEEE International Conference on Robotics and Automation (ICRA)*, Washington DC, May 12-18 2002, pp. 750–755.
- [10] C. Wilbur, W. Vorus, Y. Cao, and S. Currie, *Neurotechnology for biomimetic robots, chapter A Lamprey-Based Undulatory Vehicle*, C. London, Ed. Bradford/MIT Press, 2002.
- [11] R. Crespi, A. Badertscher, A. Guignard, and A. J. Ijspeert, "Amphibot I: an amphibious snake-like robot," *Robotics and Autonomous Systems*, vol. 50, no. 4, pp. 163–175, 2005.
- [12] A. Crespi and A. J. Ijspeert, "AmphiBot II: An Amphibious Snake Robot that Crawls and Swims using a Central Pattern Generator," in *Proc. 9th International Conference on Climbing and Walking Robots (CLAWAR)*, Brussels, Belgium, Sept. 2006, pp. 19–27.
- [13] M. Porez, F. Boyer, and A. J. Ijspeert, "Improved lighthill fish swimming model for bio-inspired robots: Modeling, computational aspects and experimental comparisons," *The International Journal of Robotics Research*, vol. 33, no. 10, pp. 1322–1341, 2014.
- [14] B. Li, S. Yu, S. Ma, and Y. Wang, "An amphibious snake-like robot with novel gaits on ground and in water," in *Proc. IASTED International Conference Intelligent Systems and Control (ISC 2011)*, Calgary, AB, July 11-13 2011, pp. 100–105.
- [15] C. Ye, S. Ma, B. Li, and Y. Wang, "Locomotion control of a novel snake-like robot," in *Proc. IEEE/RSJ International Conference on Intelligent Robots and Systems (IROS)*, Sendai, Japan, Sept. 28-30 2004, pp. 925–930.
- [16] H. Yamada, S. Chigisaki, M. Mori, K. Takita, K. Ogami, and S. Hirose, "Development of amphibious snake-like robot ACM-R5," in *Proc. 36th International Symposium on Robotics*, Tokyo, Japan, 2005.
- [17] T. Takayama and S. Hirose, "Amphibious 3d active cord mechanism "helix" with helical swimming motion," in *Proc. IEEE/RSJ International Conference on Intelligent Robots and Systems (IROS)*, Lausanne, Switzerland, Sept. 30-Oct. 2 2002, pp. 775 – 780.
- [18] C. Stefanini, S. Orofino, L. Manfredi, S. Mintchev, S. Marrazza, T. Assaf, L. Capantini, E. Sinibaldi, S. Grillner, P. Wallen, and P. Dario, "A novel autonomous, bioinspired swimming robot developed by neuroscientists and bioengineers," *Bioinspiration & Biomimetics*, vol. 7, no. 2, p. 025001, 2012.
- [19] P. Liljebäck, Ø. Stavdahl, K. Pettersen, and J. Gravdahl, "Mamba - a waterproof snake robot with tactile sensing," in *Proc. International Conference on Intelligent Robots and Systems (IROS)*, Chicago, IL, Sept. 14-18 2014, pp. 294–301.
- [20] J. Sverdrup-Thygeson, E. Kelasidi, K. Y. Pettersen, and J. T. Gravdahl, "Modeling of underwater swimming manipulators," in *Proc. 10th IFAC Conference on Control Applications in Marine Systems (CAMS)*, Trondheim, Norway, Sept. 13-16 2016.
- [21] —, "A control framework for biologically inspired underwater swimming manipulators equipped with thrusters," in *Proc. 10th IFAC Conference on Control Applications in Marine Systems (CAMS)*, Trondheim, Norway, Sept. 13-16 2016.
- [22] E. Kelasidi, K. Y. Pettersen, and J. T. Gravdahl, "Energy efficiency of underwater snake robot locomotion," in *Proc. 23th Mediterranean Conference on Control Automation (MED)*, Torremolinos, Spain, June 16-19 2015, pp. 1124 – 1131.
- [23] —, "Energy efficiency of underwater robots," in *Proc. 10th IFAC Conference on Manoeuvring and Control of Marine Craft (MCMC)*, Copenhagen, Denmark, Aug. 24-26 2015, pp. 152 – 159.
- [24] —, "Stability analysis of underwater snake robot locomotion based on averaging theory," in *Proc. IEEE International Conference on Robotics and Biomimetics (ROBIO)*, Bali, Indonesia, Dec. 5-10 2014, pp. 574–581.
- [25] E. Kelasidi, P. Liljebäck, K. Y. Pettersen, and J. T. Gravdahl, "Experimental investigation of efficient locomotion of underwater snake robots for lateral undulation and eel-like motion patterns," *Robotics and Biomimetics*, vol. 2, no. 1, pp. 1–27, 2015.
- [26] E. Kelasidi, M. Jesmani, K. Y. Pettersen, and J. T. Gravdahl, "Multi-objective optimization for efficient motion of underwater snake robots," in *Proc. The First International Symposium on Swarm Behavior and Bio-Inspired Robotics (SWARM)*, Japan, Oct. 28-30 2015, to appear in *Artificial Life and Robotics*.
- [27] Marine cybernetics laboratory (MC-lab). [Online]. Available: <http://www.ntnu.no/imt/lab/cybernetics>
- [28] Qualisys—motion capture systems. [Online]. Available: <http://www.qualisys.com>
- [29] E. Kelasidi, P. Liljebäck, K. Y. Pettersen, and J. T. Gravdahl, "Innovation in underwater robots: Biologically inspired swimming snake robots," *IEEE Robotics Automation Magazine*, vol. 23, no. 1, pp. 44–62, 2016.
- [30] Multimeter FLUKE289. [Online]. Available: <http://www.fluke.com/fluke/r0en/digital-multimeters/advanced-multimeters/fluke-289.htm?pid=56061>